การประชุมวิชาการเครือข่ายวิศวกรรมเครื่องกลแห่งประเทศไทยครั้งที่ 17
15-17 ตุลาคม 2546 จังหวัดปราจีนบุรี

การศึกษาเชิงตัวเลขของอิทธิพลของไทรโบโลยีต่อประสิทธิภาพในการตัด

Numerical study of tribological effects of machining performance

สุรังศี เดชเจริญ[1*]
ภาควิชาวิศวกรรมการผลิต คณะวิศวกรรมศาสตร์ สถาบันเทคโนโลยีพระจอมเกล้าพระนครเหนือ
1518 ถ.พิบูลสงคราม เขตบางซื่อ กรุงเทพฯ 10800
โทร 0-29132500 ต่อ 8208 โทรสาร 0-22587-4350 E-mail: surang@kmitnb.ac.th

Surangsee Dechjarem
Department of Mechanical Engineering, Faculty of Engineering, King Mongkut's Institute of Technology North Bangkok[1]
1518 Pibulsongkram Rd, Bangsue Bangkok 10800 Thailand
Tel: 0-29132500 Ext. 8208 Fax: 0-2587-4350, E-mail: surang@kmitnb.ac.th
Department of mechanical engineering, Imperial college of Science, Technology and Medicine, London, UK

Abstract

Machining tool wear is greatly affected by the tribological conditions at the tool/chip interface since the contact pressure and temperature are very high. A multi-scale analysis of metal cutting processes has been successfully developed. Macro-scale finite element models of the machining process, which included the effect of strain hardening and temperature softening, has been constructed to investigate the effect of friction on cutting parameters. The macro-scale simulation results were then used in the meso-scale finite element models of sliding contact between coated rough tool surfaces and chips. The meso-scale model demonstrated the effect of friction on the amount of material transferred from chip on to the tool by assuming ratcheting wear. The meso-scale analysis results depend on the value of ductility, but nevertheless, the trend agreed well with the experimental results.

1. Introduction

Sliding contact between tool and chip plays a very important role in cutting tool life. Large amounts of workpiece material would be transferred onto the tool surface. These severe contact conditions lead to tool wear or even rapid fracture. Therefore, it is crucial to study the tool/chip sliding contact. In this work, the mechanics of metal cutting using a coated carbide tool are examined using multi-scale analysis [1]. In this paper, a meso-scale analysis of the tool/chip sliding contact, which includes the effect of surface topography on the formation of wear debris from chip, is presented.

Sliding wear was originally explained based on adhesion theory. More recently, wear debris was observed to take the form of thin platelets resulting from the repeated unidirectional pushing of plastic waves by a hard wedge [2,3,4]. It was shown that after a small number of wave passes, crack-like features are formed and propagated by a ratcheting process. It was concluded that the surface layer is weakened and hence fails by a combination or one of ratcheting and low cycle fatigue [5,6]. In the case of low cycle fatigue, the strain cycle is normally closed and there is no accumulation of unidirectional strain. In the case of ratcheting strain, there is an accumulation of unidirectional strain in the wave formation process. In the ratcheting region, local failure is controlled by the accumulation of plastic strain measured per cycle and failure occurs when the accumulated plastic strain reaches the ductility of the material [5,7,8,9]. The use of a ratcheting wear as the criterion for the formation of debris from chips is investigated in this work.

2. Development of mesoscopic analysis of tool/chip sliding interface

2.1 Geometry and boundary conditions

In the macroscopic analysis of metal cutting, it was assumed that the nominal contact area extends over the sticking and slipping regions [1]. In this case, the actual contact area is smaller than the nominal due to the nature of the contact

introduced by the surface asperities of a real surface. The real contact area therefore covers only a fraction of the coating surface. This is illustrated in figure 1.

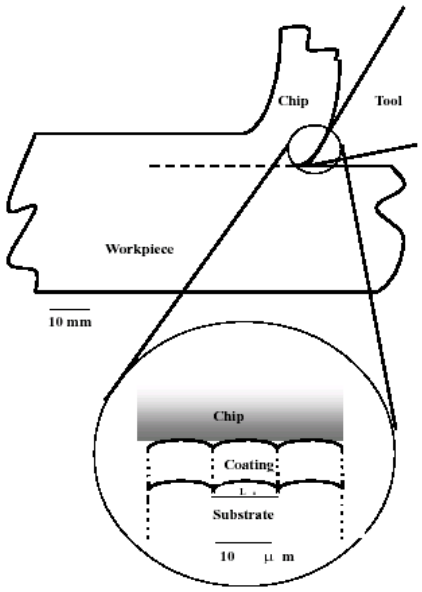

Figure 1: Illustration of the real area of contact

It has been suggested that the interaction between two rough surfaces can be modelled by a rough surface contacting a smooth one. Therefore, in this work, the topography of the coating and substrate is idealized as periodically arranged identical sinusoidal asperities, and the chip perfectly smooth, as depicted in Figure 2. The tool surface roughness is represented as periodic with mean spacing (wavelength), R_{sm} and the RMS amplitude of R_q. Therefore, as shown in Figure 2, the problem may be analyzed using a unit cell of width $2L_u$, where $L_u = R_{sm}$, and amplitude, d, where $d=4/3R_q$.

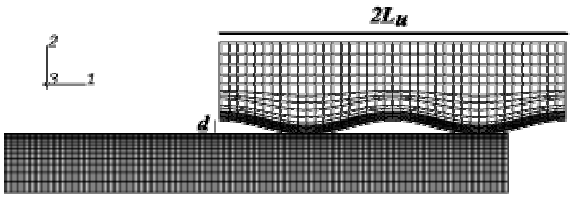

Figure 2: FE mesh of meso-scale tool/chip contact model

During the process of the chip sliding across the tool rake face, it was assumed that each asperity transfers the same contact load. The influence of the adjacent material on the deformation of the unit cell is accounted for through the use of periodic boundary conditions on the unit-cell boundaries. Thus the deformation of each point on the left hand vertical boundary must follow that of the right hand vertical boundary. The same concept applies to both the workpiece and the coated tool bodies. The tool was modelled with 1340 four-node plane strain elements. The coating was modelled with 250 plain strain elements. The workpiece however, was modelled with 1350 plain strain elements. Several surface roughness were investigated. The size of the mean spacing, R_{sm} varied from 25 to 160 μm. The size of the R_q varied from 0.30 to 7.50 μm. Ten different finite analyses were carried out with a fixed coating thickness of 4 μm. The summary of unit cell dimensions, L_u/d, used are shown in Table 2.

2.2 Material properties

The properties of the work-piece material (AISI steel) and substrate (tungsten carbide) are assumed to be the same as those used in the macroscopic analysis [1]. The workpiece is assumed to be a rate dependent, Mises material with isotropic hardening and thermal softening. A Young's modulus of 380 GPa, and a Poisson's ratio of 0.25 were used for the TiN coating [10]. Additional material properties for TiN are summarized in Table 2.

Table 1: Flow stress and equivalent plastic strain of TiN

Coating material, TiN		
Temperature (^{O}C)	Flow stress, σ (Mpa)	Plastic strain, ε_{∞}^{p}
25	1550	0.000
	1750	0.003
	1850	0.199
	2000	0.398

2.3 Contact model and conditions

The predicted contact tractions, which were used in this meso finite element analysis, were obtained from the macro-model of the cutting process [1]. The total contact load per unit out of plane thickness, F_t, the tool/chip contact length, l, the chip sliding speed, V_c and the chip maximum temperature, T_{max} were obtained from the macro-model (Table 1). The normal and tangential contact distributions acting on a coating system are taken care of by the sinusoidal surface model. The frictional contact at the interface between the tool and the chip is described by a modified-Coulomb's law.

Table 2: Surface roughness dimensions and contact conditions

surface	L_u (μm)	d (μm)	μ	F_t (N)	l (μm)	V_c (ms^{-1})	T_{max}(C)
1	150.50	6.8	0.2	202.5	2.5	65.7	582.5
2	130.53	5.3	0.2	213.7	2.5	62.9	585
3	125.48	5.5	0.2	218.5	2.4	64.3	590
4	116.75	6.5	0.2	210.0	2.0	72.7	593
5	97.8	4.6	0.2	223.5	2.1	71.4	595
6	94.3	3.8	0.2	228.4	2.1	74.1	601
7	88.5	3.4	0.2	257.5	2.6	58.2	605
8	80.0	2.1	0.2	265.0	2.7	56.5	610
9	75.8	1.9	0.2	267.5	2.7	55.6	608
10	75.8	1.7	0.2	262.5	2.4	56.9	609

3. Modelling the formation of debris from the chip

Figure 3 shows an example of the distribution of the accumulated plastic strain, ε_e, normalized by the material ductility, ε_f, at a sliding distance of $0.8L_u$, $1.5L_u$ and $1.8L_u$. It can be seen that the value of plastic strain, ε_e accumulates as the sliding continues. The maximum ε_e, starts on the chip surface and extends deep underneath the contact asperity, towards the location of maximum shear strain, ε^p_{12}, as the sliding continues. After a sliding distance of $1.8L_u$ the value of ε_e reached the material ductility, ε_f and elements failed by ratcheting. This formation of a wedge-like build-up of material ahead of the asperity is torn off to produce a wear particle.

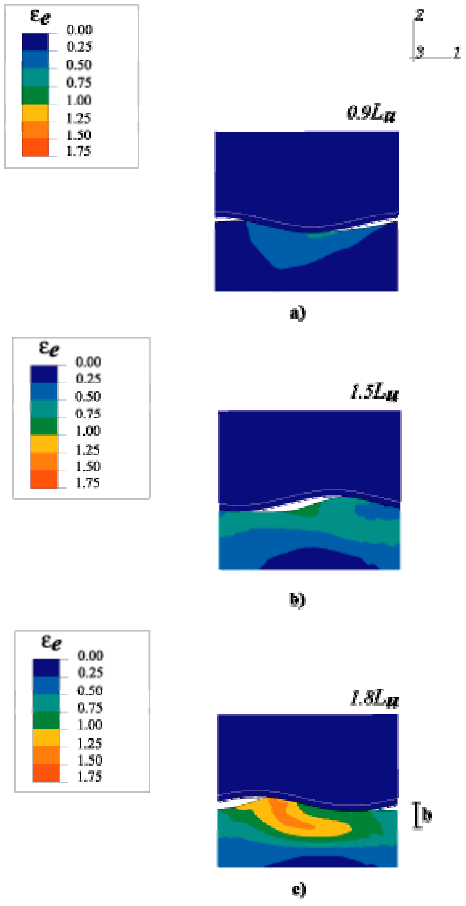

Figure 3: Typical distribution of ε_e at the sliding distance of a) 0.8Lu, b) 1.5Lu, c) 1.8Lu

Figure 4 shows the general variation of the plastic strain components, ε^p_{11}, ε^p_{22} and ε^p_{12} during the sliding at the depth, b, from the contact surface. It is clear that both the normal and shear strains components increases as the sliding continues and the value of plastic shear strain, $\varepsilon^p_{12,}$ is the highest of all components. Both phenomenon indicate ratcheting wear [8]. For ratcheting, the local failure of the material can be assumed to occur by a ductile fracture mechanism linked to the exhaustion of the local ductility of the material. In such cases, local failure maybe controlled by the accumulation of an appropriate plastic strain measured per cycle with failure occurring when it reaches the uniaxial equivalent ductility of the material. The ratcheting strain, $\Delta\varepsilon_e$, can be calculated by

$$\Delta\varepsilon_e = \varepsilon_e^{n+1} - \varepsilon_e^n \quad (1)$$

where n is number of cycles and ε_e is an effective plastic strain defined as

$$\varepsilon_e = \sqrt{\frac{2}{3}\varepsilon_{ij}^p . \varepsilon_{ij}^p} \quad (2)$$

Here, ε^p_{ij} are the components of the current plastic strain tensor and the sum is implied for i, j =1,3 [11].

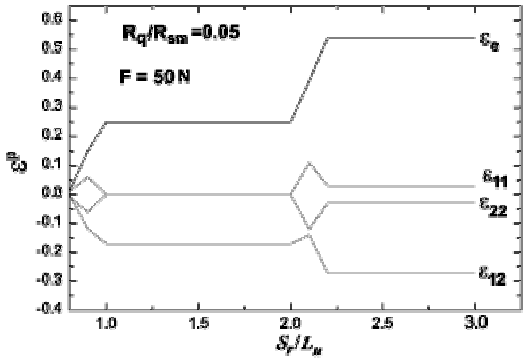

Figure 4: An example of plastic strain history at the depth b during the sliding contact of a rough surface, R_q/R_{sm}=0.05

An example of the normal plastic strain, ε^p_{22} and ratcheting strain cycle, $\varepsilon_{e,}$ experienced as material passes through the wave is presented in Figure 5. It is clear that the change in value of ratcheting strain within the second cycle is higher than the first cycle. This is thought to be the result of temperature softening. In the case of the formation of debris in metal cutting with high temperature, the effect of thermal softening is more significant than the strain hardening since material does not go through many cycles prior to the formation of debris before the chip leaves the tool surface. Therefore, the increase in value of ratcheting strain is expected to increase with sliding cycle (within the tool/chip contact length). Thus it will be assumed here for simplicity that a quasi-steady state between hardening-softening mechanisms is archived at the second cycle. The change in effective plastic strain, ε_e, within the second cycle shall be used for calculating the number of cycles required for the formations of wear debris.

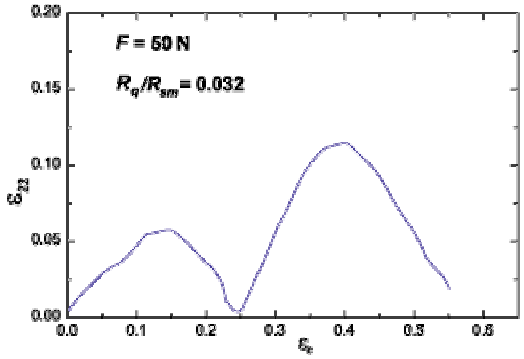

Figure 5: Ratcheting strain, ε_e and normal plastic strain, $\varepsilon_{22,}$ cycle during the sliding of rough surface contact

The number of cycles to failure due to ratcheting, which occurs when the ratcheting strain reaches the ductility, ε_f is

$$N_f = \frac{\varepsilon_f}{\Delta\varepsilon_e} \tag{3}$$

The ductility of the material, i.e. strain at fracture, is typically depends on the local stress triaxiality. In this study, the ductility is taken as 2.0, which is the value suggested by Strenkowski and Carrol (1989) and Kapoor (1994) [12,6] for AISI steel and is the same value used in the macro-scale FE model of machining for the chip separation criterion [1].

The sliding distance required prior to the formation of wear, S_r, can be calculated by

$$S_r = N_f L_u \tag{4}$$

In a machining process, the chip is only in contact with the tool surface for a certain distance before it leaves the tool surface. Hence, the index of the amount of debris transferred from the chip, *v*, during sliding contact with the tool can be calculated by

$$v = \frac{l}{S_r} \tag{5}$$

It can be seen from Figure 3 that the values of accumulated effective plastic strain, $\varepsilon_{e,}$ is the highest at the depth *b* for each surface roughness. Therefore the thickness of the removed layer (wear debris thickness), is equal to *b*, the depth of the maximum ε_e. The value of the ratcheting strain, $\Delta\varepsilon_e$ will be calculated at this depth, and will be used to calculate the number of cycles to wear debris formation. Therefore, before leaving the tool surface, the volume of wear debris transferred per unit thickness in one periodic cell of length, L_u from the chip is

$$\omega_c = vbL_u \tag{6}$$

The wear rate, w', defined as the volume of material transferred per unit width and sliding distance, here is equal to the tool/chip contact length, *l,* and can be calculated from,

$$\omega' = \frac{\omega_c}{l} \tag{7}$$

This model will be used to investigate the effect of surface roughness on the amount of wear debris transferred onto the tool surface and the results will be compared with the wear rates measured by Dechjarern [1].

4. Effect of surface roughness

4.1 Real area of contact

The real area of contact is determined by plotting the contact pressure along the contact surface. The real area of contact is then defined by the total distance where the contact pressure is higher than zero. Figure 6 shows an example of the distribution of contact pressure after two contacting cycles. It can be seen that the contact pressure decreases, while the real contact area, A_r, increases with the sliding cycle due to plastic deformation of the softer surface, i.e. AISI 4340 steel. The results agrees well with previous works [e.g. 2, 13].

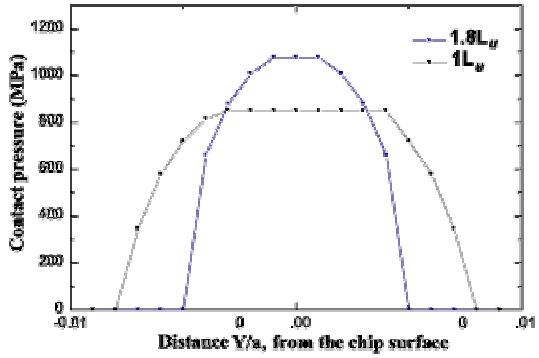

Figure 6: Contact pressure distribution on the tool surface at the sliding distance of $1L_u$, $1.8L_u$

The conformity index, ψ_c, which is the ratio of the real area of contact, A_r and the nominal area of contact, A_n, can be defined as $\psi_c = A_r/A_n$. The conformity index is an important factor in rough surface contact since conformity leads to an increase in contact area and adhesion. Figure 7 shows the variation of the conformity index, ψ_c, with the surface roughness ratio, R_p/R_{sm}. It can be seen that the conformity, decreases with surface roughness for $R_p/R_{sm} < 0.05$, after which it starts to increase slightly. The decrease in contact areas with surface roughness, R_p/R_{sm} agrees well with previous works [e.g. 14, 2, 13]. The results show that the real area seems to depend on R_p/R_{sm}, and not on the individual values of R_q or R_{sm}. For small R_p/R_{sm}, there exists a

small but finite value of R_p/R_{sm} below which the real area approaches the nominal area. For large R_p/R_{sm}, the contact is predominately plastic, mostly on the asperity peaks. The increase of contact area for surface roughness $R_p/R_{sm} > 0.05$, is thought to be the result of the increase in the spacing parameter, R_{sm}. In the present work, the spacing parameters as well as the amplitude parameter, R_q, increase with the surface roughness ratio, R_p/R_{sm} since it is the characteristics of surfaces created by EDM. As the sliding distance increases the real area of contact increases due to the plastic deformation of the chip. The results show that there may be a range of surface roughness ratio, R_p/R_{sm}, where the conformity index, ψ_c is minimum, and that many surface contact conditions can be related to the ratio R_p/R_{sm}.

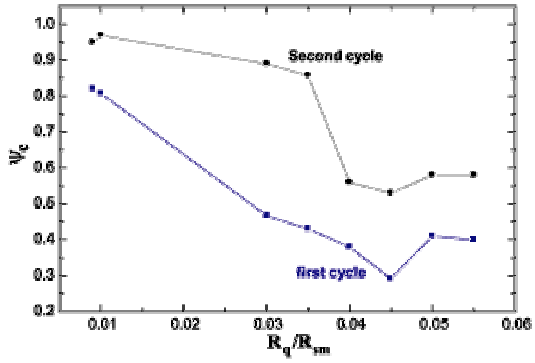

Figure 7: Variation of conformity index, ψ_c with surface roughness ratio

4.2 Formation of wear debris from the workpiece material

Figure 8 shows the variation of the wear debris thickness, *b*, with surface roughness. It appears also that the wear thickness, *b*, also increases with the ratio, R_p/R_{sm} due to the increase in plastic deformation.

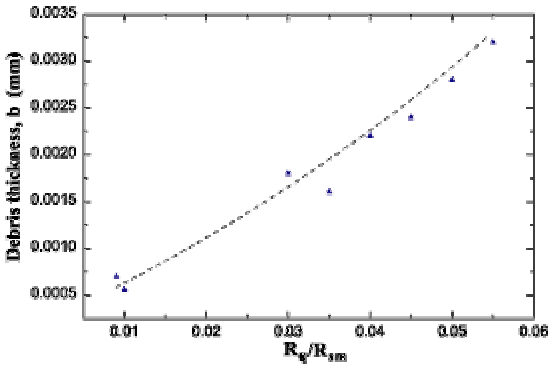

Figure 8: Variation of the debris thickness with surface roughness ratio, R_p/R_{sm}, under a load of F= 50 N and μ = 0.2

Figure 9 shows the number of cycles to failure, N_f, against surface roughness. It can be seen that the rougher the surface the lower the number of cycles needed to create the wear debris. However, in this study, the rougher surface exhibits longer spacing between asperities. Both number of cycles and surface spacing must be taken into account to predict the total amount of wear debris being created before the chip leaves the tool surface as discussed earlier. Figure 10 shows the variation of sliding distance required prior to the formation of wear debris, S_r with surface roughness ratio, R_p/R_{sm}. It is evident that the smooth surfaces ($0.03 < R_p/R_{sm} < 0.04$) require the shortest sliding distance, S_r, to create wear debris. It then appears that the value of S_r depends on surface roughness, R_p/R_{sm}, which in turn effect number of cycle to failure, N_f.

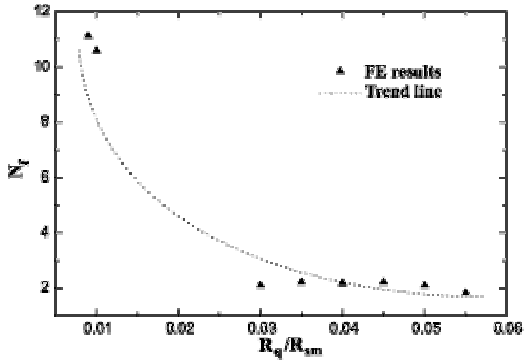

Figure 9: Variation of the number of cycle to failure, N_f with surface roughness ratio, R_p/R_{sm}, for F= 50 N and μ = 0.2

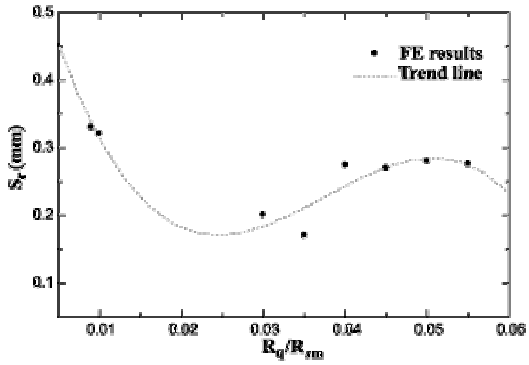

Figure 10: Variation of the sliding distance to failure, S_r with surface roughness ratio, R_p/R_{sm}, for F= 50 N and μ = 0.2

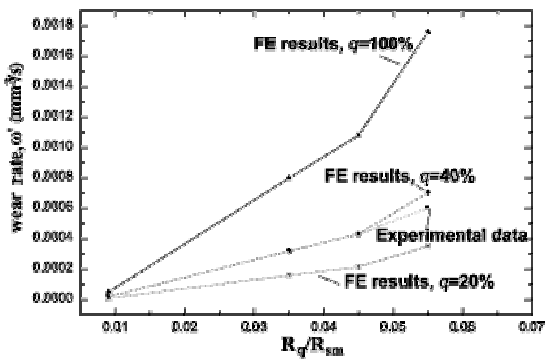

Figure 11: Variation of the rate of wear debris transferred, *w'*, with surface roughness ratio, R_p/R_{sm}, F= 50 N and μ = 0.2

Using a contact width of 2 mm, the the rate of wear debris transferred from the chip, *w'*, was calculated for different R_p/R_{sm}. Figure 11 shows the variation of the predicted wear rate, *w'*, with R_p/R_{sm} and the experiment results obtained at a sliding distance of 50 m are also plotted for comparison. In general, the rate of wear debris transferred from the workpiece increases with the surface roughness ratio. FE predictions show the same trend as that of the experimental results [1]. However, some of the wear debris predicted by FE model will be removed with chips and some may never been transferred from the chips as is the case in the experiments. The FE prediction should be multiplied by *q*, which is the percentage of remaining wear debris on tool surfaces. In the case of *q*=100%, the FE results overestimates the experimental results because the large amount of debris taking away from the tool/chip interface by the chip was not taken into account of. For *q*= 20%, the FE results underestimate the experimental results since not as much as 80% of debris was taken away from the tool/chip interface by the chip. If *q* is 40% then the FE prediction agrees well (within 5%) with experimental results.

5. Conclusions

At the meso-scale, finite element analyses were carried out to investigate the effect of surface topography, i.e. roughness ratio, R_p/R_{sm}, on the tool/chip sliding contact. The initial conditions were obtained from the macroscopic analysis of metal cutting process. Ratcheting wear was found to be the wear mechanism used to explain the process of debris transferred from the chip since the numerical results showed that both unidirectional and shear strain increase during the sliding of chips on tools. The chip failed when its accumulated ratcheting strain reached the ductility value.

The conformity index, ψ_c, which indicates the real area of contact, was found to increase with surface roughness for $R_p/R_{sm} < 0.05$, and increase slightly for $R_p/R_{sm} > 0.05$. The real area of contact, A_r, increases with sliding distance due to plastic deformation. However, the increase in contact area is lower for the rougher surfaces since plastic deformation may already take place at the early stage.

The thickness of wear debris was found to increase with surface roughness, R_p/R_{sm}, but the sliding distances required prior to the formation of debris decrease with surface roughness ratio, R_p/R_{sm}. Overall, the amount of debris transferred from the chip to the tool surface increases with R_p/R_{sm}. The mesoscopic analysis results are dependent on the value of the ductility and the percentage of remaining debris, *q,* but nevertheless, the trend agrees well with the experimental results. The results show that contact conditions can be related to the ratio R_p/R_{sm}.

References:

[1] Dechjarern S., Study of the friction and wear behavior pf a coated cutting tool with different surface topologies. Ph.D thesis, 2002, Imperial College of Science, Technology and Medicine, London, UK.

[2] Suh N. P. (1986), Tribophysics

[3] Johnson K.L., Contact mechanics, Cambridge University press, 1985, ISBN: 0521255767.

[4] Hockenhull B.S., Kopalinsky E.M., Oxley P.L.B. ,An investigation of the role of low cycle fatigue in producing surface damage in sliding metallic friction, Wear, 1991, Vol 148(1), p.135-146.

[5] Yang Y., Torrance, A., Oxley, Modelling mechanical wear processes in metallic sliding friction, Journal of applied physics, 1996, Vol 29, p600-608.

[6] Kapoor A., A re-evaluation of the life to rupture of ductile metals by cyclic plastic strain, Fatigue Fracture. Engineering Material Structure, 1994, Vol 17:2, p.201-219.

[7] Kapoor A., Johnson K.L. Plastic ratchetting as a mechanism of erosive wear, Wear, 1997, Vol 186-187, p.86-91.

[8] Yan W., O'Dowd N.P., Busso E.P., Numerical study of sliding wear caused by a loaded pin on a rotating disc Journal of the Mechanics and Physics of Solids, 2002, Vol 50, p.449-470.

[9] Oxley P.L.B., Mechanics of machining, Horwood, 1989, ISBN: 0745800076.

[10] Larsson M., Bromark, M. and Hogmark, S., Mechanical and tribological properties of multi-layers PVD TiN/NbN coatings, Surface and coating technology, 1997, Vol.91, p.43-52.

[11] Suresh S., Fatigue of materials, Cambridge : Cambridge University Press, 1998, ISBN: 0521437636.

[12] Strenkowski J. S. and Carrol J. T., An Orthogonal metal cutting model based on an Eulerian Finite element method, Manufacturing process, Machines and Systems, Proceedings of the 13th NSF Conference on production research and Technology, 1989, Vol. 13, p.95-102.

[13] Williams, J. G. (1998), Friction and plasticity effects in wedge splitting and cutting fracture tests, journal of materials science, 1998, Vol. 33, p.5351-5357.

[14] Poon C.Y., The influence of surface topography on sliding friction and in boundary lubrication, Ph.D Thesis, 1990, Imperial college of Science, Technology and Medicine, London, UK.